Applied Energy 112 (2013) 1367–1375

Contents lists available at SciVerse ScienceDirect

Applied Energy

journal homepage: www.elsevier.com/locate/apenergy

Study on flow and heat transfer characteristics of composite porous material and its performance analysis by FSP and EDEP

Zhi-Qiang Yu, Yong-Liang Feng, Wen-Jing Zhou, Yu Jin, Ming-Jie Li, Zeng-Yao Li, Wen-Quan Tao *

Key Laboratory of Thermo-Fluid Science and Engineering, Ministry of Education, School of Energy and Power Engineering, Xi'an Jiaotong University, Xi'an, Shaanxi 710049, PR China

HIGHLIGHTS

- ▶ The turbulent flow and heat transfer for four porous materials are studied.
- ▶ The field synergy principle and entransy dissipation extremum principle are used.
- ▶ The consistency of the above two principles is demonstrated.
- ▶ The values of Nu at given T_w are larger than that of given q_w for the cases studied.

ARTICLE INFO

Article history:
Received 26 September 2012
Received in revised form 8 February 2013
Accepted 19 February 2013
Available online 3 May 2013

Keywords:
Air receiver
Composite porous material
Flow and heat transfer performance
Field synergy principle
Entransy dissipation extremum principle

ABSTRACT

In this paper, the heat transfer characteristics of porous material adopted in the receiver of a concentrated solar power (CSP) with different structure parameters are numerically investigated. The commercial software FLUENT and the user defined function program (UDF) are adopted to implement the simulation. The porous material geometry is represented by periodic structures formed with packed tetrakaidecahedron. The air flow and heat transfer characteristics under the boundary conditions of constant heat flux and constant wall temperature are studied. The field synergy principle (FSP) and the entransy dissipation extremum principle (EDEP) are used to analyze the flow and heat transfer performance of the composite porous material. From the numerical results the best composite of the porous material is obtained. The effects of different boundary conditions are revealed. It is also demonstrated that the FSP and the EDEP are inherently consistent.

© 2013 Elsevier Ltd. All rights reserved.

1. Introduction

The 21st century is the time when the science and technology are developing rapidly and the energy crisis and the environment pollution problems have been turning into the most important affairs. All countries pay their attentions to the new energy, like the wind energy, the solar energy, the water energy, the geothermic energy, and the tide energy. In the solar power generation, the main research region is the tower solar thermal power generation. In the tower power generation system, the key equipment of heat transfer is the receiver which receives the solar energy and transmits it to the heat transfer medium. In recent years, researchers have developed many highly efficient solar receivers [1–4]. Fig. 1 is the diagram of a tower concentrated solar power (CSP) system. The heat transfer medium in the tower solar receiver is air [5–8]. Fig. 2 is the diagram of the pressurized volumetric air receivers [3]. From Fig. 2 we can find that the main heat transfer component in the air receiver is the porous material (i.e., the inlet/outlet absorber in Fig. 2). The porous material has many unique advantages, such as large surface area, low density, light weight, sound insulation, and good penetrability, hence, is widely adopted as the intermedium of absorbing solar energy [9–12].

During the working process of the air receiver, the heliostat field focuses the solar light to shoot on the interior of the air receiver and the solar energy irradiates the porous material. Then the porous material absorbs the solar energy and is heated. In the receiver, when the air flows from outside through the porous material it is heated, then the heated air flows out the receiver to produce water vapor.

In the theoretical and numerical researches, the porous material structure is often simplified to ideal configuration, like a series of periodical cylinder, club, and cube [13–16]. The more complicated research models are the cube model (Dul'nev model), face center model, volume center model, Weaire–Phelan unit model, Kelvin tetrakaidecahedron model and so on [17–19]. Wu et al. [20] used the tetrakaidecahedron model and FLUENT software to predict

* Corresponding author. Tel./fax: +86 29 82669106.
E-mail address: wqtao@mail.xjtu.edu.cn (W.-Q. Tao).

0306-2619/$ - see front matter © 2013 Elsevier Ltd. All rights reserved.
http://dx.doi.org/10.1016/j.apenergy.2013.02.054

Nomenclature

d	mean cell size of the tetrakaidecahedron unit (mm)
L_s	length of column framework in tetrakaidecahedron unit (mm)
d_s	diameter of column framework in tetrakaidecahedron unit (mm)
ε	porosity
ρ	fluid density (kg m^{-3})
c_p	specific heat of the fluid (J kg^{-1} K^{-1})
u	fluid velocity in the x direction (m s^{-1})
v	fluid velocity in the y direction (m s^{-1})
T	temperature (K)
Nu	Nusselt number
Re	Reynolds number
Pr	Prandtl number
β	angle of the field synergy (°)
$\overline{U}$	dimensionless velocity
$\overline{T}$	dimensionless temperature
$\bar{y}$	dimensionless coordinate y
ΔE	entransy dissipation (W K)
Q	heat transfer rate (W)
ΔT_m	temperature difference of heat transfer (K)
s	surface area of the porous material (m^2)
V	volume of heat transfer (m^3)
A	area (m^2)
h	heat transfer coefficient (W m^{-2} K^{-1})
l	characteristic length (mm)
m	mass flux (kg)
Δe	entransy flux dissipation (W K m^{-2})
q	heat flux (W m^{-2})
R	thermal resistance of heat transfer (K m^2 W^{-1})
η	fluid dynamic viscosity (kg m^{-1} s^{-1})
λ	fluid thermal conductivity (W m^{-1} K^{-1}) coefficient
ν	fluid kinematic viscosity (m^2 s^{-1})

Subscript

s	solid
w	solid wall
x	coordinate x
∞	far-field region
t	thermal boundary layer
h	heat
m	mean value
a	air
tr	heat transfer
in	inlet
i	certain point of the calculation region
p	per
E	entransy

the convection heat transfer coefficient between the air and porous foam ceramic. From the calculation results, the relationships between the porosity, air velocity, unit size, temperature and the convection heat transfer coefficient were obtained. Petrasch et al. [21,22] used computed tomography (CT) method to get the true net characteristics of porous foam and numerically simulated the penetrability and interface heat transfer performance. The tetrakaidecahedron model can present the major structure characteristics of the usual porous material quite well, and can be adequately numerically simulated. So the tetrakaidecahedron model is used in this paper for the porous material study.

As indicated above the porous material has an advantage of large ratio of surface area over volume, which is an important way for enhancing heat transfer. In the study of enhancement mechanism of convective heat transfer, researchers have made big progress. Guo et al. [23–25] revealed the physical mechanism of single phase convection heat transfer and presented the field synergy principle (FSP) between velocity and temperature gradient field. According to the FSP, the intensity of fluid convective heat transfer is not only affected by the velocity and temperature gradient, but also is influenced by the synergy degree between the velocity vector and fluid temperature gradient [26]. The FSP is tested and verified via a lot of numerical calculations and experiments [27–32]. It can unify all existing mechanisms for enhancing single phase convective heat transfer [28]. The FSP can provide a guidance for the study of enhancing convective heat transfer.

There are two irreversible processes in the convection heat transfer: momentum transfer and heat transfer. The irreversibility of the momentum transfer leads to the viscosity dissipation, and then the irreversibility of the heat transfer would bring some kind of dissipation. From the irreversibility of the thermodynamics, Bejan [33,34] suggested that the entropy generation is used to evaluate the irreversible performance of convection heat transfer. He pointed out that the minimum total entropy generation can be used to optimize convection heat transfer process. This is called the thermodynamic optimization. It is well-known that the entropy and entropy generation are the physical quantities that indicate the ability of transforming thermal energy to work. The minimum entropy generation is the object function of optimization which can be applied for energy conversion—from thermal energy to work.

To explore the object function of optimizing heat transfer process, Guo et al. [35] presented a new physical quantity—entransy. Its physical meaning is the ability of a body to transfer its internal energy (heat) to the environment. In the heat transfer process, the

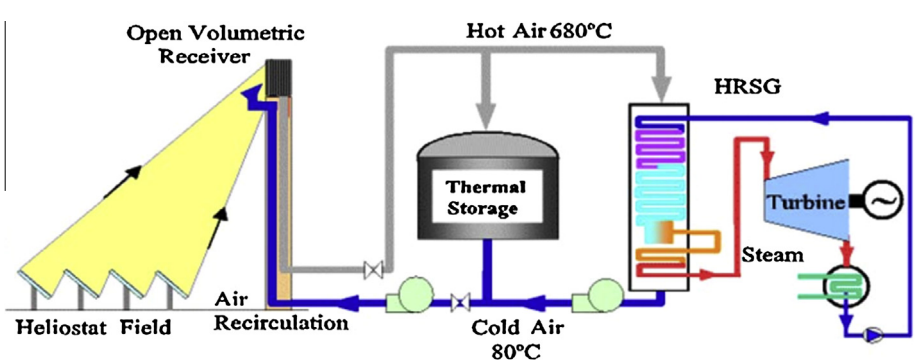

Fig. 1. Tower CSP system diagram.

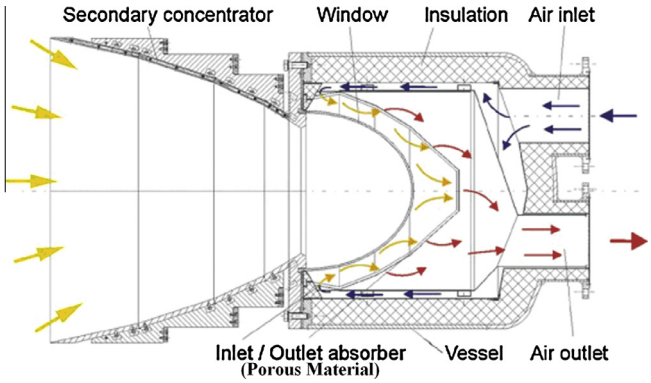

Fig. 2. Pressurized volumetric air receiver.

energy is conserved, while the ability of transferring heat is reduced because of the thermal resistance. That is to say, there is entransy dissipation in the heat transfer process. The entransy dissipation reflects the loss of heat transfer ability caused by the irreversibility in the heat transfer process. Guo et al. proposed an entransy dissipation extremum principle (EDEP) [35]. Since then the concept entransy and the EDEP have been widely adopted to analyze heat transfer problems. Cheng et al. [36] applied the EDEP in the distribution optimization of high thermal conductivity materials in the conduction process, and they obtained the optimization result superior to that obtained from minimum entropy generation principle. Meng et al. [37,38] used the EDEP and the variation method to get the optimum velocity field in the laminar flow heat transfer. Wu et al. [39] presented the EDEP in the radiation heat transfer optimization, and applied it into the radiation heat transfer between two infinite flat plates in which the emissivity optimum distribution of high emissivity material was obtained for certain conditions.

As indicated above this paper adopts the tetrakaidecahedron model to simulate the interior character of porous material. We use FLUENT software and the user-defined function (UDF) program to implement the simulation. Four different composite porous materials constituted with two different porosities are studied. The purpose of the study is to reveal the flow and heat transfer characteristics when air flows through the composite porous material. The SST k–ω turbulence model is adopted. Through numerical simulation, the air temperature, the wall temperature of the porous material and the local heat transfer coefficient between air flow and the porous material surface are obtained. For analyzing the flow and heat transfer characteristics in the four composite porous materials in depth, the FSP and EDEP are applied. Through the numerical simulation, the variations of the field synergy angle, Nu number, temperature difference of heat transfer, heat flux, entransy flux dissipation, and equivalent thermal resistance of heat transfer with the inlet Re number are obtained. As a result, we can obtain the best composite form which is superior to other three composites in the flow and heat transfer performance. It is also demonstrated that the FSP and the EDEP are consistent. In addition, the effect of different thermal boundary condition is studied in the flow and heat transfer performance research. The research results are of importance in the design of porous material used in the air receiver.

2. Introduction to FSP and EDEP

For the readers convenience the major ideas of FSP [23–25] and EDEP [35,40] are briefly presented in this section. Integrating the 2-D boundary-layer energy equation:

$$\rho c_p\left(u\frac{\partial T}{\partial x}+v\frac{\partial T}{\partial y}\right)=\frac{\partial}{\partial y}\left(\lambda\frac{\partial T}{\partial y}\right) \tag{1}$$

along the thermal boundary thickness and noting that at outside boundary the temperature gradient is zero, we obtain:

$$\int_0^{\delta_t}\rho c_p\left(u\frac{\partial T}{\partial x}+v\frac{\partial T}{\partial y}\right)dy=-\lambda\left.\frac{\partial T}{\partial y}\right|_w \tag{2}$$

In above formula, δ_t is the thermal boundary layer thickness of the two-dimensional laminar flow. Noting that the convection terms in the parenthesis of Eq. (2) is the dot production of velocity and temperature gradient, we have:

$$\int_0^{\delta_t}\rho c_p(U\cdot\nabla T)dy=-\lambda\left.\frac{\partial T}{\partial y}\right|_w \tag{3}$$

The non-dimensional form of Eq. (3) is:

$$\mathrm{Nu}_x=\mathrm{Re}_x\mathrm{Pr}\int_0^1(|\overline{U}|\cdot|\nabla\overline{T}|\cdot\cos\beta)d\bar{y} \tag{4}$$

In the above formula, $\overline{U}=U/U_\infty$, $\nabla\overline{T}=\nabla T/[(T_\infty-T_w)/\delta_t]$, $\bar{y}=y/\delta$, $T_\infty>T_w$, β is the angle between the velocity vector and temperature gradient (synergy angle). It can be found that the heat transfer rate is not only determined by the velocity, temperature difference, but is also influenced by the synergy angle between velocity and temperature gradient.

In order to optimize heat transfer process correctly, Guo et al. proposed the new parameter entransy and presented the EDEP [35]. The EDEP includes the minimum entransy dissipation principle (MINEDP) for the constant heat flux boundary condition and the maximum entransy dissipation principle (MAXEDP) for the constant wall temperature boundary condition. The MINEDP says that for given constant heat flux condition the temperature difference of heat transfer is the minimum when the entransy dissipation of heat transfer process is the minimum. Its expression for heat conduction process is

$$\dot{Q}_h\delta(\Delta T)=\delta\int_V\frac{1}{2}k(\nabla T)^2dV=0 \tag{5}$$

In the above formulation, δ is the variation symbol, ΔT is the temperature difference of heat transfer, and $\dot{Q}_h$ is the heat flux. The MAXEDP says that for given conduction temperature difference the heat flux is the maximum when the entransy dissipation is the maximum. Its expression for heat conduction process with given temperature difference is:

$$\Delta T\delta\dot{Q}_h=\delta\int_V\frac{1}{2}k(\nabla T)^2dV=0 \tag{6}$$

The meaning of the EDEP is that the maximum performance of heat transfer can be obtained when the entransy dissipation acquires the extremum. Chen et al. presented the concept of heat flux-weighted average temperature and heat flux-weighted average temperature difference in the heat transfer system [41]. They inferred the relationship of the entransy dissipation, heat flux-weighted average temperature difference and total heat flux in the condition of steady state and ignoring viscosity dissipation as follows:

$$\Delta E=\Delta T_m\cdot Q \tag{7}$$

where ΔT_m is the heat flux-weighted average temperature difference. It equals to the heat transfer temperature difference when the temperature difference can be confirmed easily, such as the logarithmic mean temperature difference $\Delta T_m=(T_{\max}-T_{\min})/\ln(T_{\max}/T_{\min})$ for conventional heat exchanger. For porous materials the difference between the area-weighted average temperature of porous material framework wall and volume-weighted average temperature of air in the total heat transfer space is adopted as such heat flux-weighted average temperature difference, that is:

$$\Delta T_m = \frac{1}{s}\iint_s T_w\,ds - \frac{1}{V}\iiint_V T_a\,dV \tag{8}$$

This paper applies the EDEP to analyze the heat transfer process. For the given constant heat flux boundary condition, the paper adopts the MINEDP to analyze the process. The evaluation indicators are the heat transfer temperature difference ΔT_m, entransy flux dissipation Δe, and the equivalent thermal resistance of heat transfer R_E. For the given temperature difference condition the wall boundary temperature and the inlet fluid temperature are given. The outlet fluid temperature is decided by the process and cannot be given in advance. So the evaluation indicators in the MAXEDP case are the heat flux q_p, the entransy flux dissipation Δe_p for 1 K temperature difference between the wall and the fluid, and equivalent thermal resistance of heat transfer R_E.

Followings are the formulas adopted in data reductions of our numerical results:

$$\Delta T_m = \frac{1}{s}\iint_s T_w\,ds - \frac{1}{V}\iiint_V T_a\,dV \tag{9}$$

$$h = \frac{Q}{\Delta T_m A_{tr}} \tag{10}$$

$$\mathrm{Nu} = \frac{hl}{\lambda} \tag{11}$$

$$\mathrm{Re} = \frac{u_{in} l}{\nu} = \frac{\rho u_{in} l}{\eta} \tag{12}$$

$$\beta_i = \cos^{-1}\left|\frac{u_i \frac{\partial T_{ai}}{\partial x} + v_i \frac{\partial T_{ai}}{\partial y} + w_i \frac{\partial T_{ai}}{\partial z}}{|\overrightarrow{U_i}||\nabla T_{ai}|}\right| \tag{13}$$

$$\beta = \frac{\sum \beta_i\,dV_i}{\sum dV_i} \tag{14}$$

$$m = \rho V = \rho u_{in} A_{in} \tag{15}$$

$$\Delta E = \Delta T_m \cdot Q \tag{16}$$

$$\Delta T_m = \frac{\Delta E}{Q} \tag{17}$$

$$\Delta e = \Delta T_m \cdot q \tag{18}$$

$$q_p = \frac{\Delta E}{\Delta T_m \cdot A_{tr} \cdot \Delta T_m} \cdot \Delta T_{mp} \tag{19}$$

$$\Delta e_p = \Delta T_{mp} \cdot q_p \tag{20}$$

$$R_E = \frac{\Delta E \cdot A}{Q^2} \tag{21}$$

In the above formulas, the air thermal conductivity λ is the volume averaged value of fluid region. The characteristic length l is the mean cell size of the tetrakaidecahedron unit, viz. $l = d = 2.828$ mm. A_{in} is the area of inlet cross-section, A_{tr} is the area of heat transfer. Re is based on the inlet data, β_i is the local field synergy angle, β is the volume averaged field synergy angle, m is the mass flux, ΔE is the entransy dissipation, Δe is the entransy flux dissipation, q_p is the heat flux for 1 K temperature difference of heat transfer, Δe_p is the entransy flux dissipation for 1 K temperature difference of heat transfer, and R_E is the equivalent thermal resistance of heat transfer.

3. The physical and mathematical models

The adopted tetrakaidecahedron model for simulating the structure of porous material is shown in Fig. 3, where d is the mean cell size of the tetrakaidecahedron unit, L_s is the length of column framework. and d_s is the diameter of column framework. In this paper, we adopt $d = 2.828$ mm and $L_s = 1$ mm. Then the porosities of the two porous materials can be calculated as follows:

(1) Dense Porous Material (DPM), $d_s = L_s/2 = 0.5$ mm, $\varepsilon = 0.8285$.
(2) Sparse Porous Material (SPM), $d_s = L_s/5 = 0.2$ mm, $\varepsilon = 0.9690$.

Because of the symmetry feature of the porous material structure, the calculation domain is selected as one circulation region of the porous material interior. For the DPM and SPM each three period lengths are elected. From the two specified porous materials there are four different composites: dense–dense (D–D), dense–sparse (D–S), sparse–dense (S–D) and sparse–sparse (S–S). When generating the grids of the porous materials for avoiding large skew degree in the parting grid, two factors need to be considered. The first one is that the column framework intersection of porous material should be smoothly managed. There are many methods in the smooth management. The paper uses the round chamfer method and the chamfer diameter is always 0.1–0.3 length of the column framework [13]. The second one is that a certain distance between the two porous materials should be kept. For the DPM and SPM, their grids should be generated separately.

The entire computation domain is composed of three parts: the inlet region, porous material region and the outlet region. Non-uniform grid system is used. In the inlet region grid should be positioned from coarse to fine, the grids in the porous material region is uniform and that in the outlet region should be from fine to coarse. The boundary conditions are set up as follows: velocity and temperature are specified at the inlet boundary; while pressure condition is adopted for the outlet boundary condition. The up, down, front, and behind boundary conditions are symmetry boundary condition. The boundary condition of porous material framework surface is no slip for momentum and given constant heat flux or constant wall temperature for energy. For example, the boundary conditions of the D–S are shown in Fig. 4. In the calculation model of this paper the computational region includes only the fluid part but no the solid part (column framework in the tetrakaidecahedron unit). For given wall heat flux or temperature the thermal boundary condition of the fluid has been fully specified. So, the governing equations are just used for the fluid region only. In addition, because heat transfer between the fluid and the porous material surfaces are simulated the porous medium model adopted in this paper is the so-called local thermal non-equilibrium (LTNE) model [42–44].

The flow turbulence intensity is usually very high in the porous material interior. It is always up to 60–80% [45]. In this paper, the

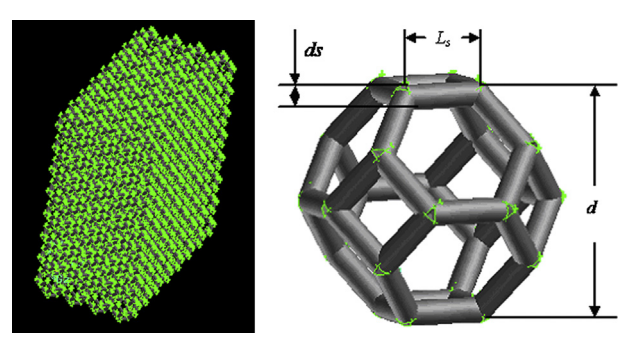

Fig. 3. Research model of porous material.

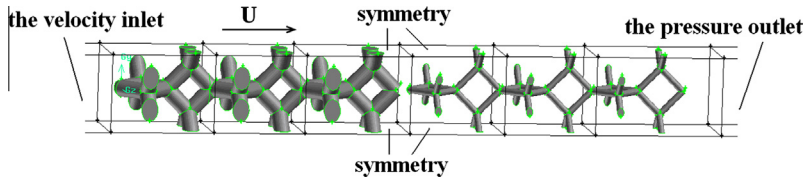

Fig. 4. Boundary condition in porous material.

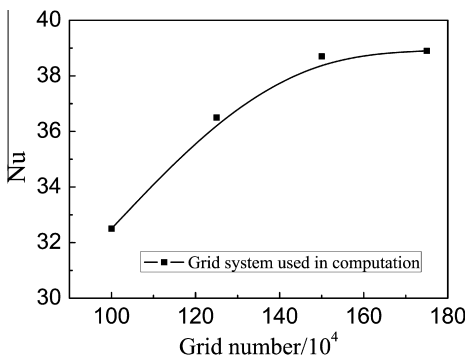

Fig. 5. Variation of Nusselt number with grid number.

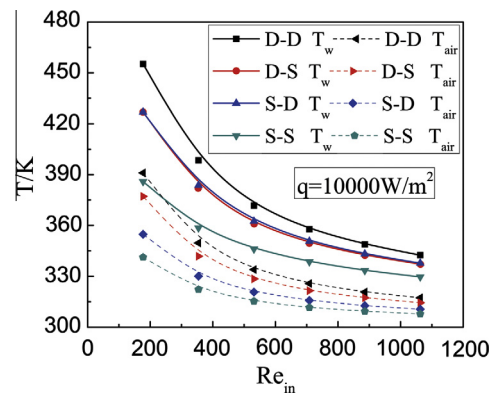

Fig. 6. Variation of wall temperature and air temperature with Re_{in}.

Re number based on the mean cell size is about 100–1000. According to Refs. [46,47], the flow is in turbulent state. Vieser and Menter used the SST k–ω model to predict heat transfer coefficient and obtained quite satisfactory results for different structural and operating parameters [48]. So, this paper adopts the SST k–ω model when predicting the turbulent flow. The air physical properties are treated as variables of the air temperature. The governing equations are the three-dimensional, steady, Reynolds-averaged Navier–Stokes equations, mass conservation and energy conservation equations, which can be found in references and textbooks [49,50], and will not be restated here. The pressure correction method SIMPLE is used in the flow field simulation [49,50]. The second-order upwind scheme is used to discretize the convection term in the momentum and energy equations [49].

The meshes of the calculation region are the tetrahedron elements and non-uniform grid system is used. For examining mesh independence of numerical solution, the calculation results of D–S are shown in Fig. 5 as an example. Through the comparison of the results, 1.5 million grids are enough for the mesh independence.

4. General numerical results

In this section, the simulation results of flow and heat transfer characteristics in the composite porous material are presented. Fig. 6 shows the variation of air bulk temperature and averaged wall temperature of porous material with the inlet Re numbers when q = 10,000 W/m^2.

In Fig. 6 it can be seen that for given constant heat flux, the sequence of porous material wall temperature is: D–D > D–S ≈ S–D > S–S. The sequence of air temperature is: D–D > D–S > S–D > S–S. The sequence of temperature difference between the wall and air is: S–D > D–D > D–S > S–S. Then the sequence of heat transfer performance is: S–S > D–S > D–D > S–D for the given heat flux boundary condition. Fig. 7 shows the variation of the cross-sectional average local heat transfer coefficient in the flow direction for q = 10,000 W/m^2 and different air inlet velocities where the inlet air temperature is 300 K.

In Fig. 7 we can find that the local heat transfer coefficient changes acutely along the flow direction. From the six cases for different combinations of heat flux and inlet velocity following features may be noted. First the local heat transfer coefficient generally decreases along the flow direction. Second, at the same position the local heat transfer coefficient increases with the inlet velocity; Third, the local heat transfer coefficient of S–S composite is the highest while that of D–D composite is the lowest; Fourth for the composites of D–S and S–D there is a turning-point of the local heat transfer coefficient variation curve, ahead and behind which the two curves change their orders. Fifth, in the downstream region of the six cases the local heat transfer coefficient of D–D case is larger than that of S–D case. Both the third and fourth features show that the heat transfer coefficient of the sparse unit is larger than that of the dense unit at the same other conditions. All the above variation trends can be well explained by FSP. In the following we take the fifth feature as an example to reveal why for both dense unit its local heat transfer coefficient is larger when it is in the D–D composite than that when it is in the S–D case.

Mathematically, the direction of temperature gradient is always perpendicular to the isothermal lines of temperature field. That is to say, where the angle between the velocity vector and isothermals is bigger where the synergy between the velocity and temperature gradient is better, which also means that the local heat transfer performance is better.

In Fig. 8 air velocity vectors and isothermals in a cross section are provided for D–D and S–D cases. In the labeled regions by red solid line of the two cases, the distributions of the isothermals are more or less the same, but the direction of velocity vector changes remarkably. In D–D case, the velocity vector and isothermals keep almost perpendicular to each other, indicating very good synergy between the velocity and temperature gradient. However, in the S–D, the angle between the velocity vector and temperature isothermals decreases, which means the synergy between the velocity and temperature gradient deteriorates. This is the reason why the local heat transfer coefficient of this region in the S–D is smaller than that in the D–D.

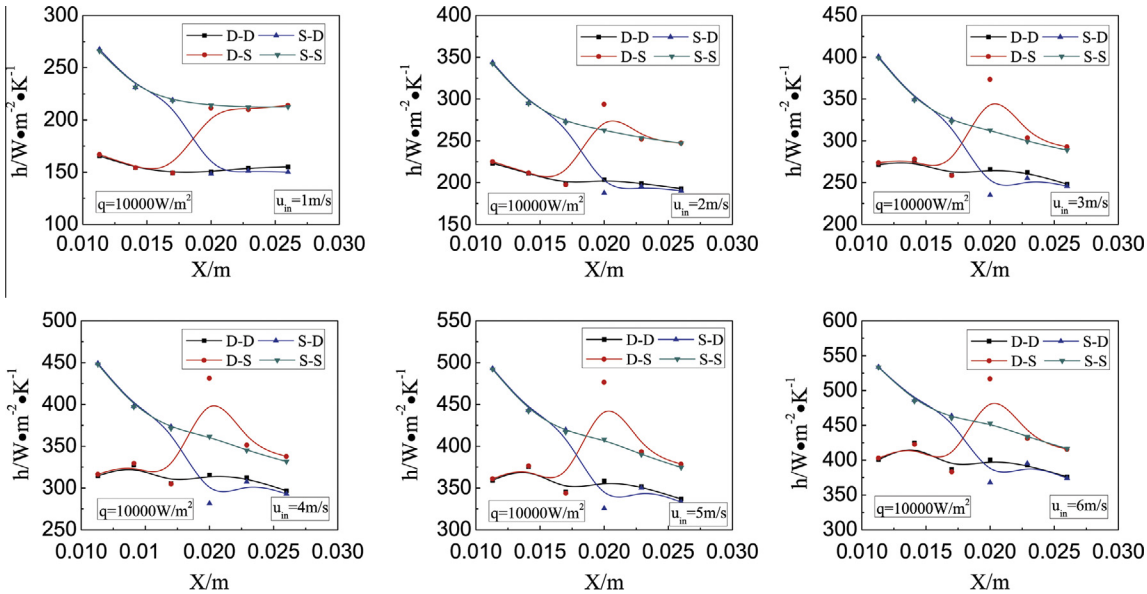

Fig. 7. Variation of local heat transfer coefficient in the flow direction.

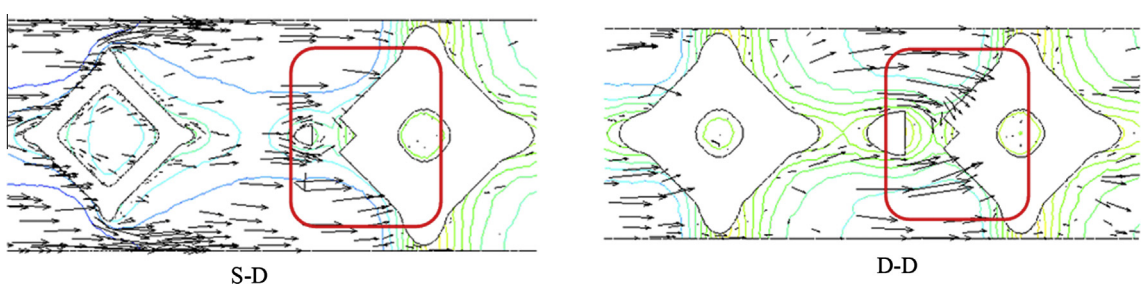

Fig. 8. Velocity and temperature fields of the two composite porous materials.

5. Results analysis for the two boundary conditions from FSP and EDSP

The numerical results for the four composite porous materials at the two boundary conditions are now analyzed and compared from points of view FSP and EDEP. The inherent connection between the FSP and the EDEP will be revealed through such analysis.

5.1. The boundary condition of constant wall temperature

The framework wall temperature of porous material is given as T_w = 500 K. The comparison is based on 1 K heat transfer temperature difference, viz. ΔT_{mp} = 1 K. Fig. 9 shows the variations of the field synergy angle, Nu number, heat flux and entransy flux dissipation, equivalent thermal resistance of heat transfer with the inlet Re number.

In Fig. 9 the sequence of field synergy angle β is: S–S < D–S < D–D < S–D. The sequence of Nu number is: S–S > D–S > D–D > S–D. The results of two evaluation indicators are agreeable.

The MAXEDP should be applied to analyze when the heat transfer temperature difference is provided. If the heat transfer performance is better, the heat flux and entransy flux dissipation are bigger and the equivalent thermal resistance of heat transfer is smaller. In Fig. 9 the sequence of heat flux q_p is: S–S > D–S > D–D > S–D. The sequence of entransy flux dissipation Δe_p is: S–S > D–S > D–D > S–D. The sequence of equivalent thermal resistance of heat transfer R_E is: S–S < D–S < D–D < S–D. The sequence of Nu number is: S–S > D–S > D–D > S–D. The results of the four evaluation indicators are agreeable, which means that the EDEP reflects the heat transfer performance exactly as that of FSP.

From the above analysis of the numerical results, it can be concluded that the FSP and EDEP are consistency in the heat transfer performance analysis of composite porous material when giving constant wall temperature.

5.2. The boundary condition of constant heat flux

For the porous material when used in the air receiver, the surface of porous material accepts the concentrated solar energy from the heliostat field. The heat flux density fluctuates violently with time.

Here we select the values of heat fluxes: q = 10,000 W/m^2 for the constant heat flux boundary condition. The heat transfer performance of porous materials is studied for the heat flux. The calculation results are shown in Fig. 10.

In Fig. 10, we can find that the variation trends of calculation results agree with each other. The sequence of field synergy angle β is: S–S < D–S < D–D < S–D. The sequence of Nu number is: S–S > D–S > D–D > S–D. The results of the two evaluation indicators are agreeable. For the boundary condition of constant heat flux the MINEDP should be applied. If the heat transfer performance is better, the temperature difference of heat transfer, the entransy flux dissipation and the equivalent thermal resistance of heat transfer are smaller. In Fig. 10 the sequence of heat transfer temperature

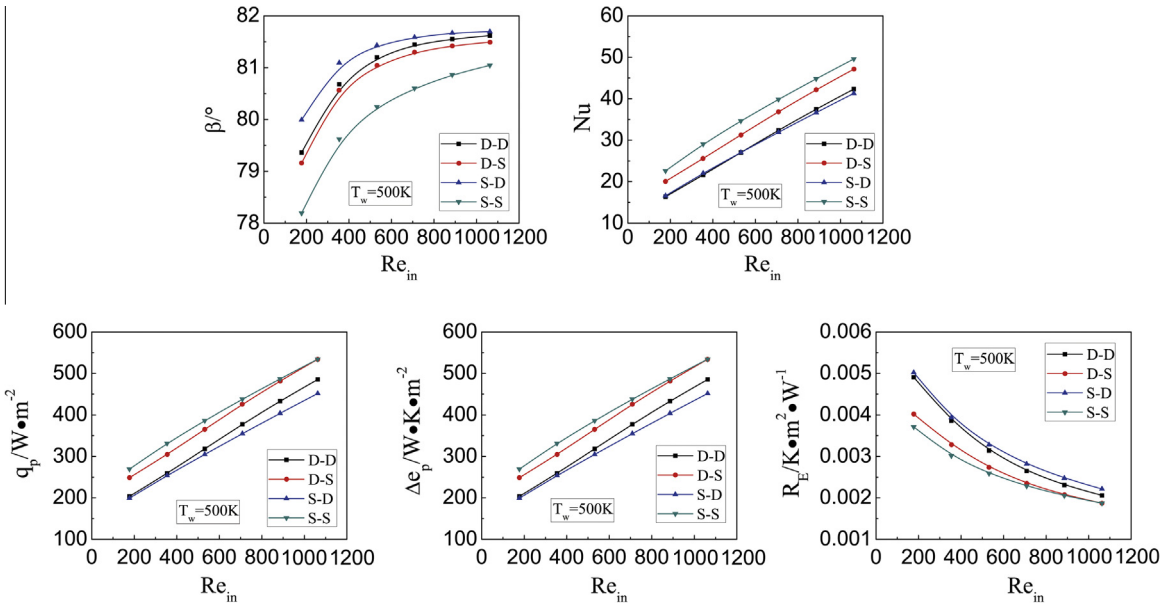

Fig. 9. Calculation results when giving constant wall temperature of 500 K.

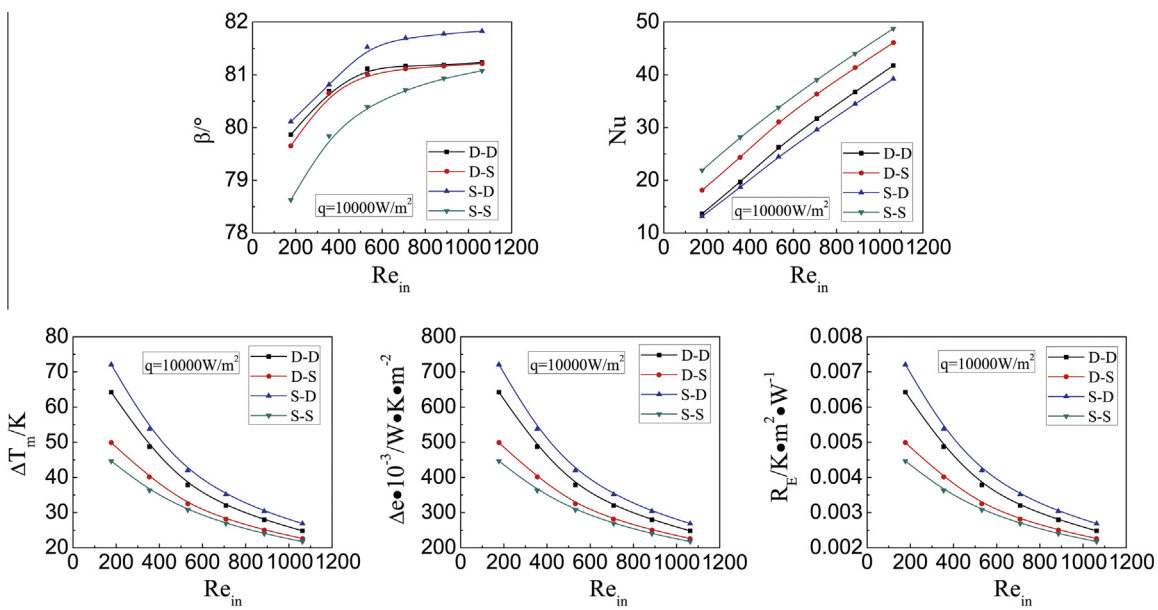

Fig. 10. Calculation results when giving constant heat flux of 10,000 W/m^2.

difference ΔT_m is: S–S < D–S < D–D < S–D. The sequence of entransy flux dissipation Δe is: S–S < D–S < D–D < S–D. The sequence of equivalent thermal resistance of heat transfer R_E is: S–S < D–S < D–D < S–D. The sequence of Nu number is: S–S > D–S > D–D > S–D. The results of the four evaluation indicators are agreeable. Once again the FSP and EDEP show their consistency for the constant heat flux boundary condition.

6. Comparison of results for two thermal boundary conditions

For the convective heat transfer of laminar flow in the pipe and trough, it is well-known that the Nu$_q$ number of the constant heat flux boundary condition is always bigger than that of the constant wall temperature boundary condition for fully developed case [51]. Guo et al. [23] used the field synergy principle to analyze this issue and found that the angle between the velocity and heat flux (i.e., temperature gradient) under the constant heat flux boundary condition is smaller than that under the constant wall temperature boundary condition. For the convective heat transfer of fully developed turbulent flow in tubes, the Nu numbers under the constant heat flux and constant wall temperature boundary conditions are approximately the same when the physical properties of fluid are constant [51].

For the situations studied in this paper whether the different thermal boundary condition affects the heat transfer performance is an interesting subject and will be discussed in this section.

To make a meaningful comparison, the two boundary conditions are compared in the following ways: (1) when giving constant heat flux boundary condition, the heat flux of the porous material framework is constant. Through the calculation, the area-weighted average temperature of porous material wall can

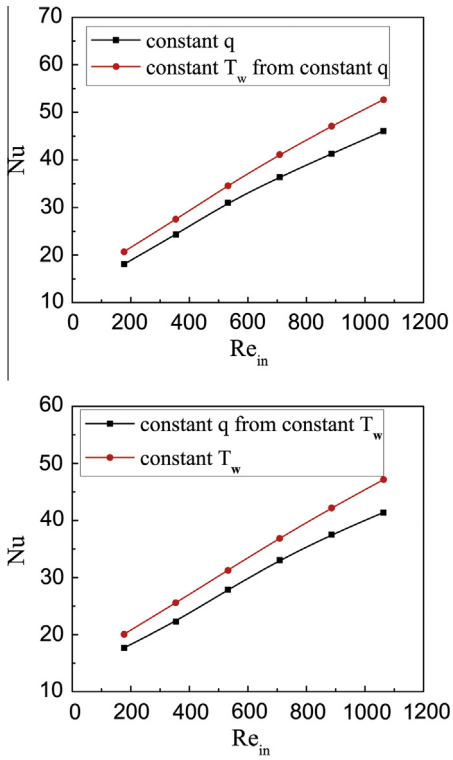

Fig. 11. Variation of Nu number with Re_{in} number at the different boundary condition.

be obtained. Then this temperature can be used as the wall temperature of porous material for the constant wall temperature boundary condition (extracted boundary condition) and (2) when giving constant wall temperature boundary condition the wall temperature of the porous material framework is constant. Through the calculation, the heat flux of the porous material wall can be obtained. Then this heat flux can be used as the heat flux of porous material for the constant heat flux boundary condition (extracted boundary condition).

For the simplicity of presentation only the comparison results for D–S composite are presented. Through the simulation, the variations of the Nu number with the inlet Re number can be obtained for giving constant heat flux and constant wall temperature boundary conditions. Here for each giving boundary condition computations are also conducted for its extracted boundary condition. The result is shown in Fig. 11. Fig. 11 shows that the Nu number in the constant wall temperature boundary condition (either original or extracted) is always bigger than that in the constant heat flux one. That is to say the heat transfer ability under the constant wall temperature boundary condition is better than that under the constant heat flux one for the situation studied.

Finally the variation characteristics of local heat transfer coefficient in the flow direction at different inlet velocities are presented in Fig. 12 for the giving constant heat flux or constant wall temperature boundary conditions. From Fig. 12 we can find that the local heat transfer coefficient under the constant wall temperature boundary condition is always bigger than that under the constant heat flux one. In addition, wave-type variations can be observed, showing the periodicity of the process.

7. Conclusions

In this paper, the flow and heat transfer performance is researched for the four composite porous materials for the constant heat flux and constant wall temperature boundary conditions. The software of FLUENT and the UDF program are used to implement the simulation. The FSP and EDEP are used to analyze the flow and heat transfer performance. From the numerical results, following conclusions can be obtained:

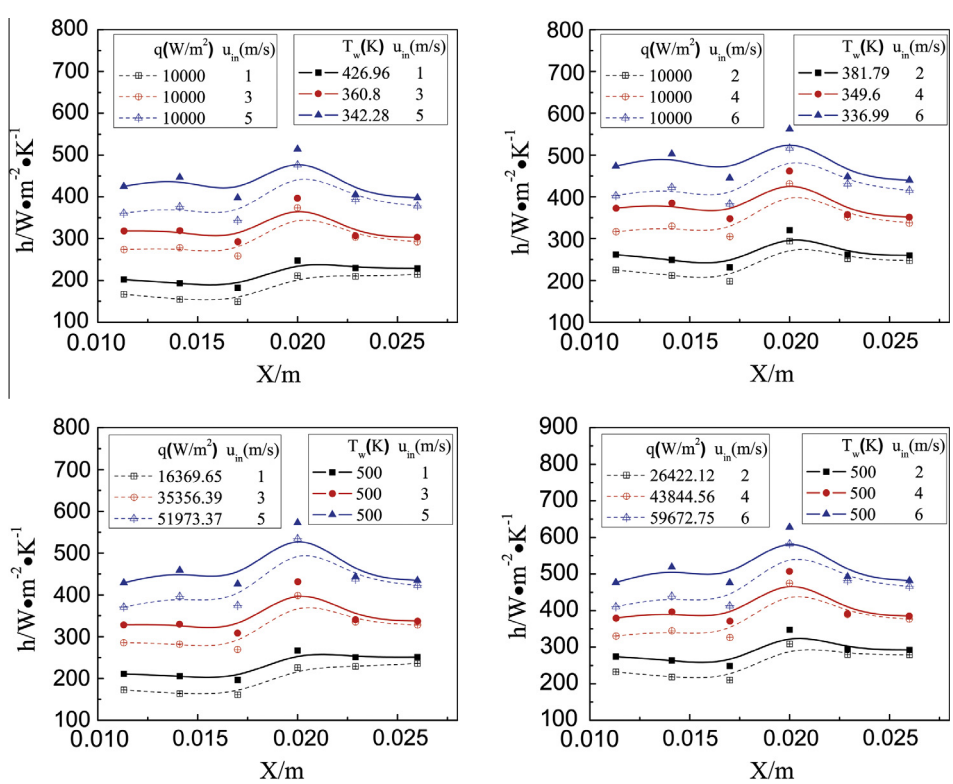

Fig. 12. Variation characteristics of local heat transfer coefficient in the flow direction.

(1) In the four composite porous materials, the order of heat transfer intensity is: S–S > D–S > D–D > S–D.
(2) In the analysis of the flow and heat transfer performance for the composite porous materials, the results analyzed from FSP and EDEP are consistent for the boundary conditions of constant heat flux and constant wall temperature.
(3) For the geometric and physical model studied, the turbulent heat transfer at given wall temperature condition is better than that of the corresponding giving heat flux condition, i.e. $Nu_T > Nu_q$.

Acknowledgements

This work is financially supported by the National Basic Key Research Program of China (G2013CB228304, G2010CB227102).

References

[1] Romero M, Buck R, Pacheco JE. An update on solar central receiver systems, projects, and technologies. J Sol Energy Eng 2002;124(2):98–108.
[2] Buck R, Brauning T, Denk T, Pfander M, Schwarzbozl P, Tellez F. Solar-hybrid gas turbine-based power tower systems (REFOS). J Sol Energy Eng 2002;124(1):2–9.
[3] Roger M, Pfander M, Buck R. Multiple air-jet window cooling for high-temperature pressurized volumetric receivers: testing, evaluation, and modeling. J Sol Energy Eng 2006;128(3):265–74.
[4] Tian Y, Zhao CY. A review of solar collectors and thermal energy storage in solar thermal applications. Appl Energy 2013;104:538–53.
[5] Fend T, Pitz-Paal R, Reutter O, Bauer J, Hoffschmidt B. Two novel high-porosity materials as volumetric receivers for concentrated solar radiation. Sol Energy Mater Sol Cells 2004;84(1–4):291–304.
[6] Becker M, Fend T, Hoffschmidt B, Pitz-Paal R, Reutter O, Stamatov V, et al. Theoretical and numerical investigation of flow stability in porous materials applied as volumetric solar receivers. Sol Energy 2006;80(10):1241–8.
[7] Fend T, Hoffschmidt B, Pitz-Paal R, Reutter O, Rietbrock P. Porous materials as open volumetric solar receivers: experimental determination of thermophysical and heat transfer properties. Energy 2004;29(5–6):823–33.
[8] Chen W, Liu W. Numerical analysis of heat transfer in a composite wall solar-collector system with a porous absorber. Appl Energy 2004;78:137–49.
[9] Oró E, de Gracia A, Castell A, Farid MM, Cabeza LF. Review on phase change materials (PCMs) for cold thermal energy storage applications. Appl Energy 2012;99:513–33.
[10] Yuan W, Tang Y, Yang X, Wan Z. Porous metal materials for polymer electrolyte membrane fuel cells – a review. Appl Energy 2012;94:309–29.
[11] Akbari MH, Riahi P, Roohi R. Lean flammability limits for stable performance with a porous burner. Appl Energy 2009;86:2635–43.
[12] Medrano M, Yilmaz MO, Nogués M, Martorell I, Roca J, Cabeza LF. Experimental evaluation of commercial heat exchangers for use as PCM thermal storage systems. Appl Energy 2009;86:2047–55.
[13] Kuwahara F, Yamane T, Nakayama A. Large eddy simulation of turbulent flow in porous media. Int Commun Heat Mass Transfer 2006;33(4):411–8.
[14] Kuwahara F, Shirota M, Nakayama A. A numerical study of interfacial convective heat transfer coefficient in two-energy equation model for convection in porous media. Int J Heat Mass Transfer 2001;44(6):1153–9.
[15] Ghosh I. Heat-transfer analysis of high porosity open-cell metal foam. J Heat Transfer 2008;130(3):034501–34506.
[16] Tzeng SC, Jywe WY, Lin CW, Wang YC. Mixed convective heat-transfers in a porous channel with sintered copper beads. Appl Energy 2005;81:19–31.
[17] Lacroix M, Nguyen P, Schweich D, Pham Huu C, Savin-Poncet S, Edouard D. Pressure drop measurements and modeling on sic foams. Chem Eng Sci 2007;62(12):3259–67.
[18] Krishnan S, Murthy JY, Garimella SV. Direct simulation of transport in open-cell metal foam. J Heat Transfer 2006;128(8):793–9.
[19] Boomsma K, Poulikakos D, Ventikos Y. Simulations of flow through open cell metal foams using an idealized periodic cell structure. Int J Heat Fluid Flow 2003;24(6):825–34.
[20] Wu ZY, Caliot C, Flamant G, Wang ZF. Numerical simulation of convective heat transfer between air flow and ceramic foams to optimise volumetric solar air receiver performances. Int J Heat Mass Transfer 2011;54(7–8):1527–37.
[21] Petrasch J, Meier F, Friess H, Steinfeld A. Tomography based determination of permeability, dupuit–forchheimer coefficient, and interfacial heat transfer coefficient in reticulate porous ceramics. Int J Heat Fluid Flow 2008;29(1):315–26.
[22] Petrasch J, Schrader B, Wyss P, Steinfeld A. Tomography-based determination of the effective thermal conductivity of fluid-saturated reticulate porous ceramics. J Heat Transfer 2008;130(3):032602–32610.
[23] Guo ZY, Li DY, Wang BX. A novel concept for convective heat transfer enhancement. Int J Heat Mass Transfer 1998;41(14):2221–5.
[24] Guo ZY, Tao WQ, Shah RK. The field synergy (coordination) principle and its applications in enhancing single phase convective heat transfer. Int J Heat Mass Transfer 2005;48(9):1797–807.
[25] Guo ZY. Mechanism and control of convective heat transfer—coordination of velocity and heat flow fields. Chinese Sci Bull 2001;46(7):596–9.
[26] Chen Q, Ren JX, Guo ZY. Fluid flow field synergy principle and its application to drag reduction. Chinese Sci Bull 2008;53(11):1768–72.
[27] Tao WQ, Guo ZY, Wang BX. Field synergy principle for enhancing convective heat transfer–its extension and numerical verifications. Int J Heat Mass Transfer 2002;45(18):3849–56.
[28] Tao WQ, He YL, Wang QW, Qu ZG, Song FQ. A unified analysis on enhancing single phase convective heat transfer with field synergy principle. Int J Heat Mass Transfer 2002;45(24):4871–9.
[29] Qu ZG, Tao WQ, He YL. Three-dimensional numerical simulation on laminar heat transfer and fluid flow characteristics of strip fin surface with *x*-arrangement of strips. J Heat Transfer 2004;126(5):697–707.
[30] Tao WQ, He YL, Qu ZG, Cheng YP. Applications of the field synergy principle in developing new type heat transfer enhanced surfaces. J Enhanc Heat Transfer 2004;11(4):435–52.
[31] Zeng M, Tao WQ. Numerical verification of the field synergy principle for turbulent flow. J Enhanc Heat Transfer 2004;11(4):453–60.
[32] He YL, Tao WQ, Song FQ, Zhang W. Three-dimensional numerical study of heat transfer characteristics of plain plate fin-and-tube heat exchangers from view point of field synergy principle. Int J Heat Fluid Flow 2005;26(3):459–73.
[33] Bejan A. A study of entropy generation in fundamental convective heat transfer. J Heat Transfer 1979;101(4):718–25.
[34] Bejan A. Entropy generation minimization: the new thermodynamics of finite-size devices and finite-time processes. J Appl Phys 1996;79(3):1191–218.
[35] Guo ZY, Zhu HY, Liang XG. Entransy—a physical quantity describing heat transfer ability. Int J Heat Mass Transfer 2007;50(13–14):2545–56.
[36] Guo ZY, Cheng XG, Xia ZZ. Least dissipation principle of heat transport potential capacity and its application in heat conduction optimization. Chinese Sci Bull 2003;48(4):406–10.
[37] Meng JA, Liang XG, Li ZX. Field synergy optimization and enhanced heat transfer by multi-longitudinal vortexes flow in tube. Int J Heat Mass Transfer 2005;48(16):3331–7.
[38] Meng JA, Liang XG, Li ZX, Guo ZY. Numerical study on low Reynolds number convection in alternate elliptical axis tube. J Enhanc Heat Transfer 2004;11(4):307–14.
[39] Wu J, Liang XG. Application of entransy dissipation extremum principle in radiative heat transfer optimization. Sci China Ser E – Technol Sci 2008;51(8):1306–14.
[40] Yuan F, Chen Q. Two energy conservation principles in convective heat transfer optimization. Energy 2011;36:5476–85.
[41] Chen Q, Ren JX. Generalized thermal resistance for convective heat transfer and its relation to entransy dissipation. Chinese Sci Bull 2008;53:3753–61.
[42] Badruddin IA, Zainal ZA, Narayana PAA, Seetharamu KN. Numerical analysis of convection conduction and radiation using a non-equilibrium model in a square porous cavity. Int J Therm Sci 2007;46:20–9.
[43] Jiang PX. Numerical simulation of forced convection heat transfer in porous plate channels using thermal equilibrium and non-thermal equilibrium models. Numer Heat Transfer, Part A: Appl 1999;35:99–113.
[44] Khashan SA, Al-Nimr MA. Validation of the local thermal equilibrium assumption in forced convection of non-newtonian fluids through porous channels. Transport Porous Med 2005;61:291–305.
[45] Hall MJ, Hiatt JP. Measurements of pore scale flows within and exiting ceramic foams. Exp Fluids 1996;20(6):433–40.
[46] Kaviany M. Principles of heat transfer in porous media. 2nd ed. New York: Springer press; 1995.
[47] Menter FR, Kuntz M, Langtry R. Ten years of industrial experience with the SST turbulence model. Heat Mass Transfer 2003;4:625–32.
[48] Tao WQ. Numerical heat transfer. 2nd ed. Berlin: Springer; 2001.
[49] Patankar SV. Numerical heat transfer and fluid flow. New York: Hemisphere; 1980.
[50] Chen Q, Ren JX. Generalized thermal resistance for convective heat transfer and its relation to entransy dissipation. Chinese Sci Bull 2008;53(23):3753–61.
[51] Yang SM, Tao WQ. Heat transfer. 3rd ed. Beijing: Higher Education Press; 2003.